HYPERSPECTRAL IMAGERY AND SPECTROSCOPY FOR MAPPING DISTRIBUTION OF HEAVY METALS ALONG STREAMLINES

Eunyoung Choe [a], Kyoung-Woong Kim [a], Freek van der Meer [b, c], Frank van Ruitenbeek [b], Harald van der Werff [b], and Boudewijn de Smeth [b]

[a] Gwangju Institute of Science and Technology (GIST), Department of Environmental Science and Engineering, 1 Oryong-dong, Buk-gu, 500-712 Gwangju, Republic of Korea.
[b] International Institute for Geo-information Science and Earth Observation (ITC), Department of Earth Systems Analysis, Hengelosestraat 99, 7500 AA Enschede, the Netherlands.
[c] Utrecht University, Department of Physical Geography, Heidelberglaan 2, 3508 TA Utrecht, the Netherlands.

E-mail: eychoe@gist.ac.kr, kwkim@gist.ac.kr, vdmeer@itc.nl, vanruitenbeek@itc.nl, vdwerff@itc.nl, desmeth@itc.nl

ABSTRACT For mapping the distribution of heavy metals in the mining area, field spectroscopy and hyperspectral remote sensing were used in this study. Although heavy metals are spectrally featureless from the visible to the short wave infrared range, possible variations in spectral signal due to heavy metals bound onto minerals can be explained with the metal binding reaction onto the mineral surface. Variations in the spectral absorption shapes of lattice OH and oxygen on the mineral surface due to the combination of heavy metals were surveyed over the range from 420 to 2400 nm. Spectral parameters such as peak ratio and peak area were derived and statistically linked to metal concentration levels in the streambed samples collected from the dry stream channels. The spatial relationships between spectral parameters and concentrations of heavy metals were yielded as well. Based on the observation at a ground level for the relationship between spectral signal and metal concentration levels, the spectral parameters were classified in a hyperspectral image and the spatial distribution patterns of classified pixels were compared with the product of analysis at the ground level. The degree of similarity between ground dataset and image dataset was statistically validated. These techniques are expected to support assessment of dispersion of heavy metal contamination and decision on optimal sampling point.

KEY WORDS: Heavy Metal, Hyperspectral Remote Sensing, Mapping, Spectral Parameter, Spectroscopy

1. INTRODUCTION

To survey the spatial distribution of heavy metals, general methods involving the systematic sampling and laboratory analysis of environmental samples follow interpolation of the point results in compiling distribution maps (Ferrier, 1999; Kemper and Sommer, 2002). Such an approach is time-consuming and costly. Remote sensing has been applied to the rapid and broad investigation of the dispersion of pollution and the use of hyperspectral data has improved upon previous results.

While heavy metals are known to be spectrally featureless from the visible to the short wave infrared range, possible variations in spectral signal due to heavy metals bound onto minerals can be explained with the metal binding reaction onto the mineral surface.

In this study, field spectroscopy and hyperspectral remote sensing are used for mapping the distribution of heavy metals in the mining area. This study focus on finding spectral parameters which can represent metal concentrations based on the heavy metal binding mechanism and comparing the spatial distribution of spectral parameters and geochemical values in the mapping results.

2. MATERIALS AND METHODS

2.1 Field Sample Analysis

2.1.1 Measurement: For the observation at the ground level, sediment samples were collected along the dry stream channel around the Au and Pb-Ag mining area. Samples were sieved in the field to obtain the fraction smaller than 2 mm. For the analysis of sediment samples, As and Zn were considered to be indicative of environmental pollution and were chemically analyzed using ICP-AES and AAS. The reflectance signal in the VNIR (visible and near-infrared) and SWIR (short wave infrared) range was measured using ASD FieldSpec Pro under laboratory conditions.

2.1.2 Derivation of Spectral Parameters: Variations in spectral absorption shapes of lattice OH and oxygen on the mineral surface due to the combination of heavy metals were surveyed over the range from 420 to 1400 nm and from 2100 to 2400 nm. Spectral parameters such as peak ratio and area were derived and statistically linked to metal concentration levels in the streambed samples collected from the dry stream channels (Figure

1). The binding reaction of metal cations (M^{2+}) on such hydroxylated surface sites (*R*OH, *R* can be Al, Fe, Mn, Si, etc.) of clay or metal oxide minerals are generally described as follows (Robert et al., 2005):

$$ROH + M^{2+} = ROM^{+} + H^{+} \quad (1)$$
$$ROH + M^{2+} = RO\text{–}M^{+} + H^{+} \quad (2)$$

The spectral features of *R*OH and *R*O (e.g., FeO) in clay and oxide minerals whose positions are assigned at around 2200 nm and from 500 to 1000 nm, respectively (Ben-Dor, 1999), may change once heavy metals are bound to the minerals.

2.2 Hyperspectral Imagery

2.2.1 Image data: The airborne imaging spectrometer HyMAP operated by HyVista Corporation was used in this study which acquired in 2004 (Figure 2). The sensors collected reflected solar radiation in 126 narrow bands over the 450–2500 nm wavelength range and with a 4 m spatial resolution. The HyMAP data was atmospherically and geometrically corrected using the ATCOR 4 model.

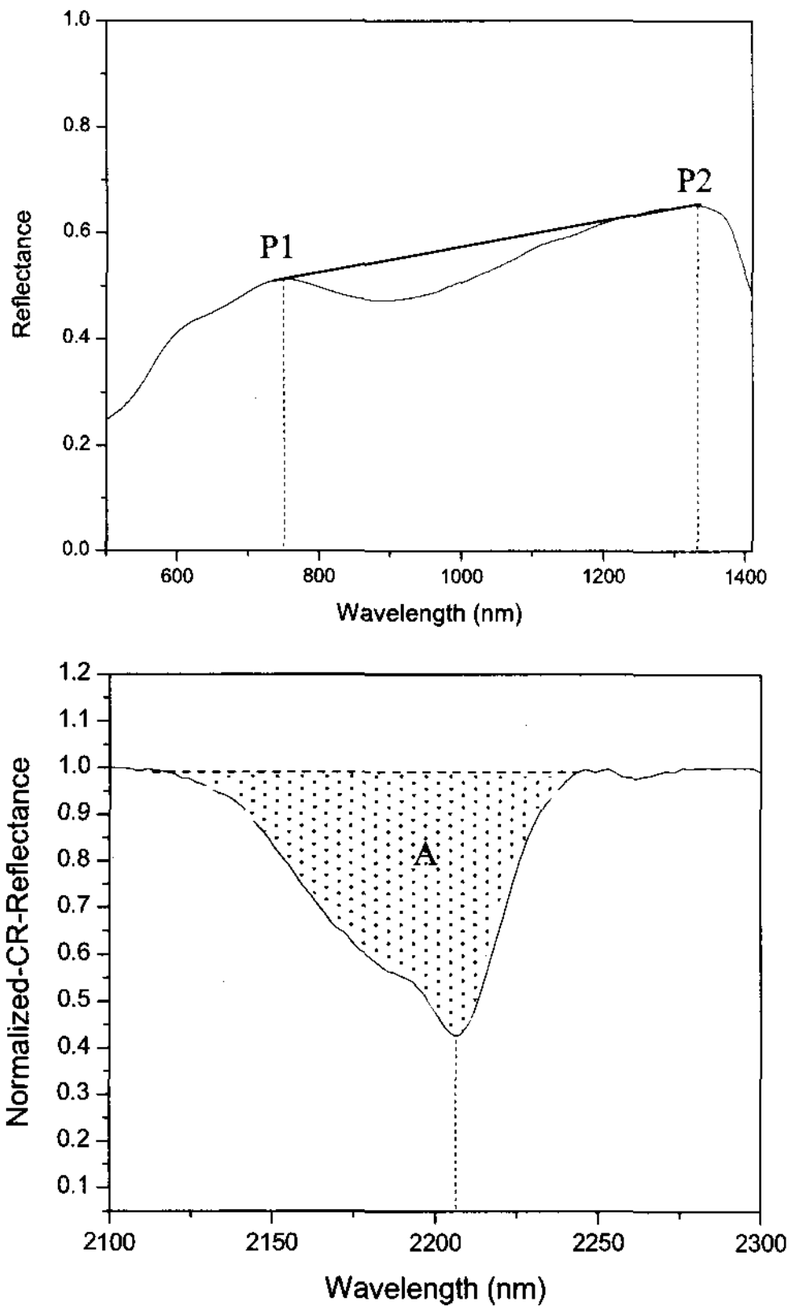

Figure 1. Variations in the spectral absorption shape in the VNIR and SWIR range. (a) Ratio of 1344 to 778 nm (P2/P1) in the VNIR region. (b) Absorption area (A) at about 2200 nm for sediment samples including 370 ppm of heavy metal.

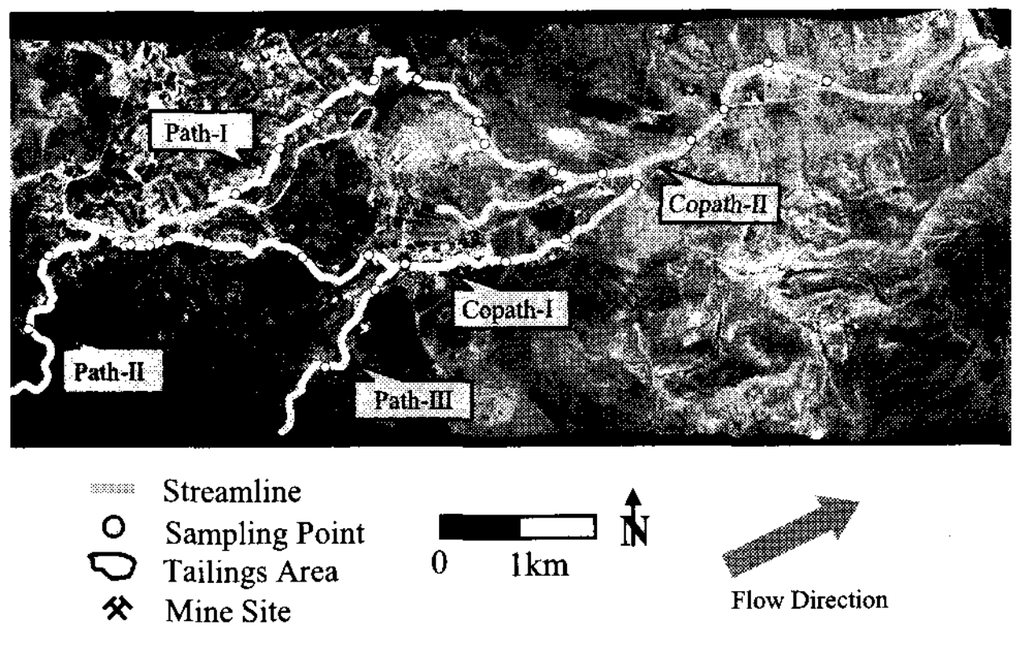

Figure 2. HyMAP^{TM} image acquired in 2004 on which landmarks for this study such as streamline and sampling points are overlaid.

2.2.2 Classification: For mapping spectral parameter using HyMAP data, image-processing techniques such as continuum-removal, normalization, and calculation of parameters were applied. A 40 m wide bufferzone from the streamline was considered as a study section to focus on the spread of pollution by stream water during the rainy season. The linking process of spectral parameters to heavy metal levels was simplified via a binary fitness function (Legg et al., 2004; Debba et al., 2005) that enables classification of areas affected by heavy metals:

$$w_s(x_{i,j}) = \begin{cases} 0, & if \;\; S(x_{i,j}) < S_t \\ 1, & if \;\; S(x_{i,j}) \geq S_t \end{cases} \quad (3)$$

where $x_{i,j}$, i = 1,2,...,n, and j = 1,2,…,m, represent the pixel spectra associated with the spatial location, i, and j, respectively, and $S(x_{i,j})$ is each spectral parameter value. A threshold (S_t) was assigned from representative values of spectral parameters determined from ground analysis.

3. RESULTS AND DISCUSSION

3.1 Relationship between Geochemical Values and Spectral Parameters

The strengths of the relationships between spectral parameters and heavy metal levels were measured using Pearson's correlation, as summarized in Table 1. Arsenic concentrations showed a statistically significant correlation with $R_{1344/778}$ at the 0.05 of *p*-value. Arsenic was paired with $R_{1344/778}$ value for comparison. The correlation between Zn level and A_{2200} in the SWIR range revealed a relatively high negative *r*-value (p = 0.001). When heavy metals combine to the surface functional group, e.g., *R*OH (Formulas 1 and 2), it is possible that the spectral absorption shape of the molecule at the assigned spectral position might weaken because of a decrease in the amount of *R*OH at the mineral surface.

Table 1. Pearson's correlations between spectral parameters and heavy metal concentrations.

Element	$R_{1344/778}$		A_{2200}	
	r-value	*p*-value	*r*-value	*p*-value
As	0.258	0.048*		
Zn			–0.438	0.001**

* Correlation is significant at the 0.05 level.

** Correlation is significant at the 0.01 level.

Although the results of Pearson's correlation was insufficient in terms of developing a quantitative model for directly predicting heavy metal concentrations from spectral parameters, the relationships indicated the potential of semi-quantitative mapping.

3.2 Comparison of Mapping Results between Ground Dataset and Image Dataset

The spectral parameter values were compared between HyMAP data and ground data in Table 2. The $R_{1344/778}$ of image dataset showed comparable patterns to the results of the ground dataset. The ANOVA results summarized in Table 3 describe the relationship between spectral parameters on the ground and those obtained from images. The *p*-values (< 0.05) and F-values (> $F_{critical}$) for A_{2200} parameter indicated a significant difference between the image and ground datasets for each of the sampling points. The one-way ANOVA within each stream section was also calculated because the populations of these parameters recorded different mean values in each stream section (Table 3). The ANOVA results in divided sections for A_{2200}, path-I and path-III exhibited no significant difference between the two populations. The F value calculated for image and ground $R_{1344/778}$ in whole area was smaller than the corresponding $F_{critical}$ (p = 0.859). It could therefore be concluded that there were no significant differences in $R_{1344/778}$ values, and that the ANOVA results for all stream sections also showed statistical similarity between two datasets. The differences in spectral parameter values between image and ground data can be explained in terms of the contrasting scales of observation (Kim and Barros, 2002).

Table 2. Comparison of mean values of spectral parameters between image dataset and ground dataset in each stream section

	Parameter	Path-I	Path-II & Copath-I	Path-III	Copath-II
Ground	$R_{1344/778}$	1.325	1.318	1.435	1.374
	A_{2200}	34.4	25.1	11.1	50.4
Image	$R_{1344/778}$	1.356	1.357	1.342	1.331
	A_{2200}	21.9	6.7	28.8	12.6

Table 3. The one-way ANOVA result between image and ground dataset for $R_{1344/778}$ and A_{2200}

Parameter	ANOVA	Path-I	Path-II & Copath-I	Path-III	Copath-II	Total
$R_{1344/778}$	F	0.705	0.048	0.035	0.264	0.032
	p-value	0.412*	0.830*	0.854*	0.626*	0.859*
	$F_{critical}$	4.414	4.747	4.747	5.987	4.020
A_{2200}	F	2.619	20.239	0.732	93.179	11.293
	p-value	0.123*	0.001	0.409*	0.000	0.001
	$F_{critical}$	4.414	4.747	4.747	5.318	4.013

* No significant differences at $p > 0.05$.

4. CONCLUSION

In this study, we focused on finding spectral parameters to represent heavy metal levels for mapping their distribution and assessing the possibility of applying the parameters to hyperspectral imagery.

Ratio of 1344 to 778 nm ($R_{1344/778}$) in the VNIR range and peak area at 2200 nm (A_{2200}) in the SWIR range were considered as the spectral parameter to enable mapping of variations associated with heavy metal concentrations. In terms of the pairs of spectral parameters and heavy metal concentrations, $R_{1344/778}$ and As and A_{2200} and Zn showed statistically significant relationships. However, the strengths of these relationships were insufficient in terms of quantitatively representing heavy metal levels based on spectral parameters. The results indicated that the spectral parameters could be used for semi-quantitative mapping of the distribution or dispersion of pollution.

For the spectral parameters calculated from HyMAP image, the spatial pattern of classified pixels in the rule images of the $R_{1344/778}$, and A_{2200} parameters was somewhat similar to the spectral parameter distribution of sediment samples. For the ANOVA result, while $R_{1344/778}$ was statistically similar in the image and ground datasets, A_{2200} was only partly similar. The different observation scales of the two datasets might explain the differences in spectral parameter values.

Although there are many complications and limitations in terms of using spectroscopy and remote sensing techniques in quantifying environmental events, these techniques are expected to support assessment of dispersion of heavy metal contamination and decision on optimal sampling point.

ACKNOWLEDGEMENTS

This work was supported by the Korean Science and Engineering Foundation (KOSEF) through the National Research Lab. program funded by the Korean Ministry of Science and Technology (No. M10300000298-06J0000-29810).

REFERENCES

Ben-Dor, E. Irons, J.R., and Epema, G.F., 1999, Soil reflectance. In A.N. Rencz (Ed.), Remote sensing for the earth sciences: Manual of remote sensing (pp. 111-188). New York: John Wiley & Sons.

Debba, P., van Ruitenbeek, F.J.A., van der Meer, F.D., Carranza, E.J.M., and Stein, A., 2005, Optimal field sampling for targeting minerals using hyperspectral data. Remote Sens. Environ., 99, pp. 373-386.

Ferrier, G., 1999, Application of imaging spectrometer data in identifying environmental pollution caused by mining at Rodaquilar, Spain. Remote Sens. Envrion., 68, pp. 125-137.

Kemper, T. and Sommer, S., 2002, Estimate of heavy metal contamination in soils after a mining accident using reflectance spectroscopy. Enrion. Sci. Technol., 36, pp. 2742-2747.

Kim, G. and Barros, A.P., 2002, Downscaling of remotely sensed soil moisture with a modified fractalinterpolation method using contraction mapping and ancillary data. Remote Sens. Environ., 83, pp. 400–413.

Legg, S., Hutter, M., and Kumar, A., 2004, Tournament versus fitness uniform selection. Technical Report IDSIA-04-04 of IDSIA (Istituto Dalle Molle di Studi sull'Intelligenza Artificiale).

Roberts, D., Nachtegaal, M., and Sparks, D.L., 2005, Speciation of metals in soils. In M.A. Tabatabai and D.L. Sparks (Ed.), Chemical processes in soils (pp. 619-654). Wisconsin: Soil Science Society of America.